Final Report

December 2018

Pressure-Based Inversion and Data Assimilation System (PIDAS) for CO_2 Leakage Detection

SUBMITTED UNDER FUNDING OPPORTUNITY ANNOUNCEMENT (FOA 0000798)

WORK PERFORMED UNDER AGREEMENT

DE-FE0012231 (10/01/2013-09/30/2018)

SUBMITTED BY

The University of Texas at Austin
Jackson School of Geosciences
Bureau of Economic Geology
University Station, Box X
Austin, Texas, 78713

DUNS #170230239

PRINCIPAL INVESTIGATOR

Alex Sun, PhD
PH: 512-475-6190
alex.sun@beg.utexas.edu

SUBMITTED TO
PROJECT MANAGER
Bruce M. Brown
Bruce.Brown@NETL.DOE.GOV

U. S. Department of Energy
National Energy Technology Laboratory

Final Report

December 2018

Pressure-Based Inversion and Data Assimilation System (PIDAS) for CO_2 Leakage Detection

Leading Authors:

Alexander Y. Sun (Principal Investigator), Jiemin Lu*, Akand Islam**, Susan Hovorka

Bureau of Economic Geology, Jackson School of Geosciences, The University of Texas at Austin

*currently at Schlumberger Inc.,
**now at Fiat Chrysler Automobiles

DISCLAIMER

ABSTRACT

This project aims to develop a Pressure-based Inversion and Data Assimilation System (PIDAS) for detecting CO2 leakage from storage formations. Carbon capture, utilization, and sequestration (CCUS) has the potential to enable deep reductions in global carbon emissions if high storage efficiency can be achieved. A major hurdle to industrial-scale implementation of geological carbon sequestration (GCS) projects is the potential migration of fluids (either brine or injected CO_2) from the storage formations and the resulting legal and financial liabilities. The capability to accurately identify leakage pathways by which stored CO2 could leak, has leaked, or is leaking from the targeted storage zone is thus of paramount importance to site licensees and regulators. Although many MVA techniques have been devised, pressure-based monitoring technology remains the most sensitive and reliable technique for early detection. Pressure-based monitoring has consistently received the highest score in terms of benefit/cost ratio and it provides the greatest potential for leakage detection with broad areal coverage. Under this project we have (a) demonstrated the utility of the proposed well testing technique for leakage detection through integrated theoretical and numerical analysis, laboratory experiments, and field tests; (b) developed effective data analysis and inversion algorithms for identifying leakage pathways by fusing data generated during well testing; (c) provided a designing tool for maximizing the utility of the developed PIDAS tool for early leakage detection.

ACKNOWLEDGMENTS

The authors would like to thank DOE NETL for funding this research and the Jackson School of Geosciences at The University of Texas at Austin for providing the cost share. We are grateful to the DOE NETL project managers, Mr. Brian Dressel and Mr. Bruce Brown, for their guidance during the project. We thank colleagues at the Gulf Coast Carbon Center at Bureau of Economic for endless insightful discussion. We acknowledge the generous assistance from Denbury Resources, Sandia Technology Inc., and Dr. Barry Freifeld and his team for making the field experiment possible.

TABLE OF CONTENTS

1. INTRODUCTION

The overall objective of this project is to develop a *Pressure-based Inversion and Data Assimilation System (PIDAS)* for detecting CO_2 leakage from geologic carbon storage (GCS) formations. Under this project, we have developed and demonstrated a cost-effective, pressure-based, harmonic pulse testing (HPT) technique for leakage detection. A multipronged research is designed and performed for this multiyear project, including numerical modeling, laboratory experiments, and field experiments.

1.1 Project objectives

A major hurdle to industrial-scale implementation of GCS projects is the potential migration of fluids (e.g., brine or injected CO_2) from the storage formations and the resulting legal and financial liabilities. The capability to accurately identify leakage pathways by which stored CO_2 could leak, has leaked, or is leaking from the targeted storage zone is thus critical to GCS site operators and regulators. Although many MVA techniques have been developed, pressure-based monitoring technology remains the most sensitive and reliable technique for early detection. It has consistently received the highest rank in terms of benefit to cost ratio and provides the greatest potential for leakage detection with relatively large areal coverage. Much has been done in the area of forward modeling of fluid migration in CO_2 storage formations in the last decades. However, the more challenging pressure anomaly inversion problem requires further theoretical, experimental, and field validation to be used effectively as a leakage detection method. In this project, a HPT well testing technique is adapted for leakage detection and additional theoretical, laboratory, and field experiments are performed to support the feasibility study.

In particular, the main research objectives of PIDAS are to

- Demonstrate the utility of the proposed well testing technique for leakage detection through integrated theoretical and numerical analysis, laboratory experiments, and field tests;
- Develop effective data fusion and inversion algorithms for identifying leakage pathways by fusing data generated during well testing;
- Design a web-based optimal well testing tool for knowledge dissemination and publish best practice procedures in peer-reviewed papers for maximizing the utility of the developed PIDAS tool for early leakage detection.

The following integrated tasks are designed to achieve the overall objective of the PIDAS project

Task 1: Project management and planning
Task 2: Theoretical development and numerical validation of harmonic pulse testing
Task 3: Laboratory experiments
Task 4: Inversion and data assimilation algorithm
Task 5: Field experiments
Task 6: Integration and reporting

1.2 Literature review

1.2.1 Pressure base leakage detection

Leakage detection is a special type of inverse problems and has long been studied by water engineers for pipeline leakage and contaminant source identification (Mahar and Datta, 2001; Mandal et al., 2012; Michalak and Kitanidis, 2004; Puust et al., 2010; Sun et al., 2006). Existing

leakage detection methods based on pressure signals can be classified broadly into time-domain and frequency-domain diagnoses.

Time-domain diagnoses inspect observed pressure time series in the time domain for potential anomalies. Methods fallen in this category can be further divided into model-driven and data driven. In model-driven methods, the source release history is first parameterized and the unknown parameters are sought by minimizing the difference between model predictions and pressure observations. In (Sun and Nicot, 2012), the performance of several inverse algorithms for identifying leakage in geologic carbon storage formations. Their approach for identifying leakage rates is based on pulse-response analysis, through which observed pressure data are deconvoluted to infer the leakage history of sources. In their work, the complicated problem of joint inversion of source locations and leakage rates is decoupled by embedding the deconvolution algorithm in a global optimization solver. In the inner loop, an inversion solver obtains the leakage history for given leak location, whereas in the outer loop, the global optimization solver attempts to identify the most probably leak locations that gives the best match with observed pressure signals. Jung et al. (2013) solved an optimization problem directly to identify both uncertain permeability values and leak locations. Potential caveats of the model-driven methods are that (a) they generally require a high-fidelity forward model that is suitable for leakage inversion; in other words, the model must be able to simulate pressure responses caused by any hypothetical leak locations during the solution process; and (b) the resulting inverse problem is ill-posed and can be easily interfered by both model uncertainties and measurement noise.

In data-driven approaches, a black-box model (e.g., artificial neural networks) is first trained offline using historical observations and then deployed online for anomaly detection. The black-box model typically consists of a forecast module that predicts the nominal system behaviors at the operational conditions, and a fault detection module that can recognize system anomalies in real time and trigger warnings. The effectiveness of such data-driven methods depends critically on past records of leakage. Because of data incompleteness and information vagueness, most methods adopt either a probabilistic or fuzzy-theoretic approach. Mandal et al. (2012) used the support vector machine (SVM) in conjunction with artificial bee colony algorithm to predict leaks in oil pipelines. Arsene et al. (2012) developed a decision support system for detecting leaks in water distribution systems based on a three-layer, fuzzy min–max neural network and graph theory. Zhang et al. (2010) applied fuzzy logic theory to estimate probability of leakage from faults, in which the leakage probability is related to domain size, CO_2 plume size, and parameters describing conduit length distribution and uncertainty. For deep subsurface monitoring and risk assessment projects, however, data-driven models can be difficult to train because of the sparsity of known leakage incidents. A possibility is to use a risk-based framework to combine model-driven and data-driven methods such that the former is used to simulate leakage events for the latter to learn (Yang et al., 2011).

Frequency domain diagnosis methods typically transform observed pressure responses using Fourier transform, and then inspect the frequency responses for possible anomalies. For linear time-invariant systems, the *frequency response function*, defined as the ratio of the Fourier spectra of output and input pressure signals, characterizes a physical system in terms of its amplitude attenuation and phase shift (see also the next subsection). The amplitude attenuation measures how much signal strength is reduced when the sourced signal reaches an observation point, while the phase shift measures how much delay the signal has experienced after traveling to the observation point. Frequency domain diagnosis has been used to detect pipeline leaks by analyzing pressure responses to pseudo-steady-state flows. In practice, oscillatory flows can be easily induced into a

problematic pipeline section by opening/closing an upstream valve periodically. The power spectra of such fluid transients are affected by pipeline anomalies (e.g., leaks and blockages), thus giving clues that can be used for locating such anomalies (Ferrante and Brunone, 2003; Lee et al., 2005; Mpesha et al., 2001). Unlike the time domain diagnoses, frequency domain diagnoses are generally less prone to interference by ambient noise and has long been used as an alternative analysis tool in reservoir characterization (see Section 1.2 below). To the best of our knowledge, frequency domain diagnosis has not been applied to leakage identification in geologic repositories; thus, its effectiveness requires a quantitative assessment, which is the main focus of this project.

1.2.2 Background on harmonic pulse testing

Harmonic pulse testing (HPT) is a well testing technique in which periodic flow rates are applied to an active well (also known as pulser) continuously until a pseudo-steady-state condition is established. The pressure responses are continuously recorded at one or more observation wells. Unlike the conventional well interference tests that are often conducted under the constant flow rates, HPT possesses the following advantages: (a) it requires much less or even zero net fluid extraction/injection; (b) the oscillating harmonic pulse signals, when analyzed in a spectral space, are easier to identify even when the background is noisy; and (c) HPT can be run with flow rates oscillating around the average production rate and thus create minimal disruption to ongoing reservoir operations. As it will be clear from the rest of this report, these advantages of the HPT make it a suitable method for leakage detection in the storage reservoir. In comparison, most of the existing pressure-based detection methods are passive monitoring methods, meaning the pressure gauges are typically deployed in a carefully selected geologic unit out of the injection zone to monitor for potential leakage signals. If the thickness of the confining unit is too large, however, the leakage pressure signals will be very much attenuated before it reaches those out-of-zone units.

The concept of pulse testing was originally introduced in 1960s (Johnson et al., 1966). It involves alternating flow and shut-in periods having constant rates and duration, whereby pressure disturbance is recorded in surrounding monitoring wells (Black and Kipp, 1981). Thus, pulse tests effectively impose a square or rectangular wave to the test formations. Traditionally, pulse tests have been primarily used in hydrogeology and petroleum engineering fields to establish communication between wells and to determine the interwell connectivity and reservoir properties, through either type curve analysis or pressure derivative analysis (Bernabé et al., 2006; Cardiff et al., 2013; Gringarten, 2008; Hollaender et al., 2002; Kuo, 1972b; Mishra et al., 2013; Rasmussen et al., 2003). Some important developments occurred during the late 1970s–1980s are the introduction of systems approach to the analysis of well tests (Gringarten, 1986; Gringarten, 1987) and the treatment of well test interpretation as a type of inverse problems. Also, it was recognized during that time that the number of possible dynamic behaviors of a reservoir is limited. The basic reservoir dynamic behavior reflects the number of different porous medium mobility and storativity in the reservoir that participate in the flow process (Gringarten, 2008). The former is defined as the ratio between permeability k and viscosity μ

$$\lambda = \frac{k}{\mu}, \tag{1}$$

whereas the latter is defined as the product of porosity ϕ and total compressibility c_t. During well tests, the basic reservoir behavior is reflected during intermediate times, whereas the near wellbore and boundary effects are reflected during early and late times, respectively.

The currently form of HPT used was originally proposed by Kuo (1972a) as an extension to (single) pulse testing. Unlike pulse tests, however, interpretation of HPT is primarily done in frequency domain.

To begin with, suppose a sinusoidal flow rate with frequency ω_0 is imposed at the injector. Here, ω_0 denotes the fundamental angular frequency, $\omega_0 = 2\pi / T$, with T the period of sinusoid. The complex pressure response at the injector due to this periodic pulse can be written as

$$p_{inj} = A_{inj} \exp[i(\omega_0 t + \theta_{inj})], \tag{2}$$

where A_{inj} is amplitude, ω_0 is angular frequency of sourcing signal, and θ_{inj} is phase. Similarly, the complex pressure response at the observation well due to the periodic pulse is

$$p_{obs} = A_{obs} \exp[i(\omega_0 t + \theta_{obs})]. \tag{3}$$

The amplitude ratio or attenuation is defined as

$$\Lambda = \frac{A_{obs}}{A_{inj}}. \tag{4}$$

The phase shift is defined as

$$\Theta = \theta_{inj} - \theta_{obs}. \tag{5}$$

Attenuation is a measure of how much the observed signal is reduced from the sourcing signal, whereas phase shift provides a measure of how much delay the signal experiences after traveling through a porous medium (Ahn and Horne, 2010). Together attenuation and phase shift characterize the frequency response of a reservoir. By definition, attenuation varies in (0,1) and phase shift can also be normalized to (0, 2π).

In practice, it is usually hard to generate a time-varying sinusoidal rate. The repeated square- or rectangular-waves may be used instead. Or, one can simply use complex rate function. In this latter case, by decomposing the sourcing signal into summation of sinusoidal waves (which is possible because Fourier expansion can be used to approximate arbitrary functions in real space), the reservoir can be systematically analyzed in the frequency domain. Let the sourcing signal (i.e., flow rate) $q(t)$ applied at the pulser well be decomposed into a sum of harmonics with different frequencies

$$q(t) = \sum_{\omega} \hat{Q}(\omega) e^{i\omega t} \tag{6}$$

where $\hat{Q}(\omega)$ is Fourier coefficient corresponding to frequency ω. For each sourcing frequency, the pressure response functions can be obtained either analytically or numerically. Previous studies suggest that signals from different sourcing frequencies can be used to reveal permeability distributions by "reflecting different radii of influence from the point of injected signal" (Ahn and Horne, 2010; Black and Kipp, 1981). This fact is one of the main promises underlying the HPT.

Analytical solutions exist for special cases. For example, Black and Kipp (1981) derived analytical solutions to aquifer pulse test for a sinusoidal perturbation in a confined non-leaky aquifer with infinite boundaries. Their starting point is the governing PDE of groundwater flow in homogeneous and isotropic media

$$\nabla^2 h(\mathbf{x},t) = \frac{S_s}{K}\frac{\partial h(\mathbf{x},t)}{\partial t} + q(\mathbf{x},t), \qquad h = h_0 \text{ when } r \to \infty \tag{7}$$

where S_s is specific storage, K is hydraulic conductivity, h is hydraulic head, and q is sink/source. An equivalent form of Eq. (7) used in petroleum engineering is hydraulic diffusivity equation, which is given in the axisymmetric form as

$$\nabla \cdot (k\nabla p) = \phi c_t \mu \frac{\partial p}{\partial t}, \tag{8}$$

where p is pressure and the meanings of other symbols are already defined around Eq. (1) in the above. Assuming homogeneous medium, then the term $k/(\phi c_t \mu)$ is known as diffusivity.

In the frequency domain, Eq. (7) becomes

$$\nabla^2 \hat{H} - i\omega S_s \hat{H} = \hat{Q} \tag{9}$$

where $\hat{H}$ and $\hat{Q}$ are the Fourier transform of h and q, respectively,

$$\hat{H}(\mathbf{x},\omega) = \frac{1}{\sqrt{T}}\int_0^T h(\mathbf{x},t)e^{-i\omega t}dt, \tag{10}$$

$$\hat{Q}(\mathbf{x},\omega) = \frac{1}{\sqrt{T}}\int_0^T q(\mathbf{x},t)e^{-i\omega t}dt. \tag{11}$$

In axisymmetric coordinates and for a periodic point source located at $r = 0$ in an infinite domain, the steady periodic solution (i.e., when pressure reaches periodic steady state) to (7) is (Black and Kipp, 1981)

$$h(r,t) = \frac{Q}{4\pi Kr}\exp\left[-\frac{1+i}{\sqrt{2}}\left(\frac{\omega S_s r^2}{K}\right)^{1/2}\right]e^{i\omega t} \tag{12}$$

for which the corresponding amplitude A and phase θ are, respectively,

$$A = \frac{Q}{4\pi Kr}\exp\left[-r\left(\frac{\omega S_s}{2K}\right)^{1/2}\right], \tag{13}$$

$$\theta = -r\left(\frac{\omega S_s}{2K}\right)^{1/2}. \tag{14}$$

The attenuation and phase shift can then be obtained as

$$\Lambda = \frac{A_{obs}}{A_{inj}} = \frac{r_w}{r_o}\exp\left[-(r_o - r_w)\left(\frac{\omega S_s}{2K}\right)^{1/2}\right], \tag{15}$$

$$\Theta = -(r_w - r_o)\left(\frac{\omega S_s}{2K}\right)^{1/2}, \tag{16}$$

in which r_w is injector radius and r_o is distance between injector and observer. Note that the ratios are independent of the rate information.

For periodic line source penetrating the entire aquifer thickness, the steady periodic equation is (Black and Kipp, 1981)

$$h(r,t) = \frac{Q}{4\pi Kl} K_0 \left[\left(\frac{\omega S r^2}{K} \right)^{1/2} e^{i\pi/4} \right] e^{i\omega t}, \quad (17)$$

where K_0 is zero-order, modified Bessel function of the second kind and l is thickness of the aquifer. The attenuation and phase shift corresponding to the line source case can be calculated (see Black and Kipp, 1981). Rasmussen et al. (2003) derived steady periodic solutions for sinusoidal pumping in a leaky aquifer and in a confined aquifer with partially penetrating well, respectively.

In most situations, however, analytical solutions are not available. Numerical models are used to solve for pressure responses at the injector and observer(s). The results are then transformed into frequency domain by using fast Fourier transform (FFT).

2. TASK 2: THEORETICAL DEVELOPMENT AND NUMERICAL VALIDATION OF HARMONIC PULSE TESTING

2.1 Theoretical analysis

The PIDAS project is built upon the harmonic pulse test (HPT) concept for leakage detection. The main hypothesis is that leakage will create disturbance in the pressure field, which in turn, will cause deviation from the baseline pressure responses. When pressure responses are examined in frequency domain, the deviations will effect either attenuation or phase shift, or both. Importantly, induced pressure perturbations is expected to be clearly discerned in the frequency domain "because all the energy of the imposed signal is concentrated in a small number of frequencies, while noise typically exhibits a broad frequency spectrum" (Fokker and Verga, 2011).

As a general rule, an effective leak detection method must be sensitive to the appearance of leaks, but insensitive (robust) to other changes, such as noise, modeling errors, and normal signal variations. In other words, the leak detection method needs to have a relatively high signal-to-noise ratio.

We consider a three-layer system consisting of a storage reservoir, an aquitard (confining layer), and an overlying aquifer (see Figure 1). For this stylized 3-layer reservoir we are able to derive semi-analytical solutions. The results presented below have been peer reviewed before (Sun et al., 2015).

The aquifer properties in each layer are assumed homogeneous. An injector is located in the origin (axisymmetric coordinates), and an observation well is located at a distance r_O away. In the leak scenario, a leaky well is present at a distance r_I from the injector and the distance between leaky well and observation well is denoted by r_L. Such a problem setting has been routinely used in analytical and numerical studies for leakage modeling (e.g., Avci, 1994; Birkholzer et al., 2011; Cihan et al., 2011; Nordbotten et al., 2004; Sun et al., 2013; Zeidouni, 2014). Most of the previous analytical studies assumed constant injection rate. An exception is the work by Cihan et al. (2011), whose semianalytical solutions can handle temporally variable injection rates by approximating the injection history using a piecewise-constant function; however, the result is less accurate than modeling the sinusoidal rate directly. Thus, we derived a semi-analytical solution for sinusoidal injection rates.

In the absence of leaks, the governing equation for pressure response in the storage reservoir (layer 1) corresponding to a source located at the origin is again the hydraulic diffusivity equation shown in the last section, but is repeated below for completeness

$$\frac{\partial^2 p}{\partial r^2}+\frac{1}{r}\frac{\partial p}{\partial r}=\frac{\phi\mu c_{t,1}}{k_1}\frac{\partial p}{\partial t} \tag{18}$$

subject to initial and boundary conditions

$$p(r,t=0)=p_{init}$$
$$\lim_{r\to\infty}p(r,t)=p_{init}$$
$$\frac{2\pi k_1 b_1}{\mu}r\frac{\partial p}{\partial r}\bigg|_{r=r_w}=-Q(t)$$

where $p=p(r,t)$ is pressure; p_{init} is the initial pressure; the injection rate $Q(t)=Q_b(t)+Q_o e^{i\omega t}$ is the sum of a non-sinusoidal regular injection term, Q_b, and a complex HPT source term, $Q_o e^{i\omega t}$, with Q_o denoting the magnitude and $\omega=2\pi/T_p$ the angular frequency corresponding to pulse period T_p; r_w is the radius of the injector; and ϕ, μ, k, b, and c_t denote porosity, fluid viscosity, permeability, layer thickness, and total compressibility, respectively. Because the pressure response caused by Q_b is an additive trend and needs to be filtered out before frequency domain analysis, in the following we shall disregard Q_b unless otherwise noted and simply focus on pressure responses resulting from the sinusoidal source term $Q_o e^{i\omega t}$. Also, we focus on the scenario that each pulse experiment only uses a single frequency, although multi-frequency experiments can be performed.

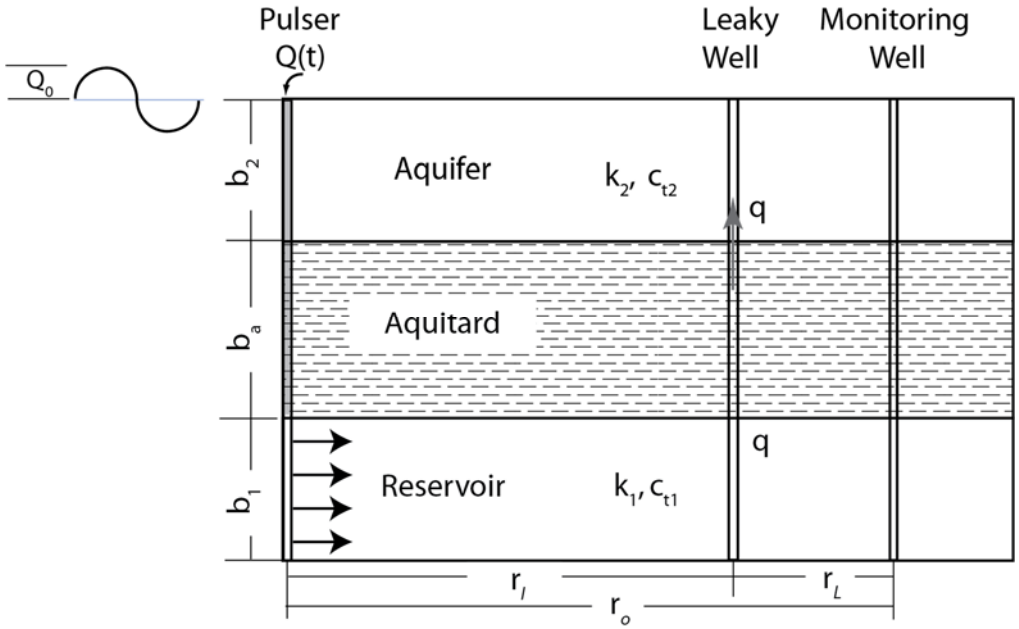

Figure 1. Schematic plot of a stylized 3-layer GCS repository consisting of reservoir, aquitard, and aquifer from bottom to top. The system has a pulser, a leaky well, and a monitoring well. The aquifer properties are assumed given and homogeneous. Distances between leaky well and pulser and between pulser and monitoring well are labeled on the figure.

The Laplace domain solution to the diffusivity equation (18) is (Sun et al., 2015)

$$\hat{P}(r) = \frac{Q_o \mu}{2\pi k_1 b_1 r_w (s - i\omega)\sqrt{s/\eta_1}} \frac{K_0(r\sqrt{s/\eta_1})}{K_1(r_w\sqrt{s/\eta_1})}, \tag{19}$$

in which r is the distance between injector and an arbitrary observation location; s is the Laplace transform variable; K_0 and K_1 are the zeroth- and first-order modified Bessel function of the second kind, respectively; $\eta = k/\phi\mu c_t$ is diffusivity; and $\hat{P}$ is the Laplace transform of the pressure buildup $p - p_{init}$.

When a leak is present, the Laplace-transformed pressure buildup in the reservoir is

$$\hat{P}_{1,l}(r_l) = \frac{\hat{q}\mu}{2\pi k_1 b_1 r_a \sqrt{s/\eta_1}} \frac{K_0\left(r_l\sqrt{s/\eta_1}\right)}{K_1\left(r_a\sqrt{s/\eta_1}\right)}, \tag{20}$$

in which r_l is the distance between the leak well and an arbitrary observation location, r_a is radius of the leak well, and $\hat{q}$ is Laplace transform of the leakage rate. Thus, the Laplace transform of total pressure buildup in the reservoir, p_1^T, is the sum of Eqs. (19) and (20)

$$\hat{P}_1^T = \hat{P} + \hat{P}_{1,l}. \tag{21}$$

Similarly, the Laplace-transformed total pressure buildup in the upper aquifer caused by the leak is

$$\hat{P}_2^T(r_l) = -\frac{\hat{q}\mu}{2\pi k_2 b_2 r_a \sqrt{s/\eta_2}} \frac{K_0\left(r_l\sqrt{s/\eta_2}\right)}{K_1\left(r_a\sqrt{s/\eta_2}\right)}. \tag{22}$$

The Laplace transform of the unknown leakage rate can then be expressed using Darcy's law,

$$\hat{q} = -\frac{k_a \pi r_a^2}{\mu}\left(\frac{\hat{P}_2^T - \hat{P}_1^T}{D_l}\right), \tag{23}$$

where D_l is the vertical length of the leakage pathway from the reservoir to the upper aquifer, k_a is the associated permeability, and the system is assumed to be at hydrostatic equilibrium initially. Solving for $\hat{q}$ from Eqs. (19)–(23) gives

$$\hat{q} = \frac{\dfrac{-Q_o K_0(r_l\sqrt{s/\eta_1})}{2\pi k_1 b_1 r_w (s - i\omega)\sqrt{s/\eta_1} K_1(r_w\sqrt{s/\eta_1})}}{\Omega + \dfrac{K_0(r_a\sqrt{s/\eta_1})}{2\pi k_1 b_1 r_a \sqrt{s/\eta_1} K_1(r_a\sqrt{s/\eta_1})} + \dfrac{K_0(r_a\sqrt{s/\eta_2})}{2\pi k_2 b_2 r_a \sqrt{s/\eta_2} K_1(r_a\sqrt{s/\eta_2})}}. \tag{24}$$

where both $\hat{P}_1^T$ and $\hat{P}_2^T$ are evaluated at the wellbore of the leaky well (i.e., $r_l = r_a$), and the flow resistance term is $\Omega = D_l/(\pi r_a^2 k_a)$. A complete solution including the effect of Q_b is given in Appendix B of (Sun et al., 2015) . From Eq. (24), it is straightforward to obtain the Laplace transformed total pressure buildups in both the reservoir and the upper aquifer,

$$\hat{P}_1^T = \frac{\hat{q}\mu}{2\pi k_1 b_1 r_a \sqrt{s/\eta_1}} \frac{K_0(r_L\sqrt{s/\eta_1})}{K_1(r_a\sqrt{s/\eta_1})} + \frac{Q_o\mu}{2\pi k_1 b_1 r_w (s-i\omega)\sqrt{s/\eta_1}} \frac{K_0(r_O\sqrt{s/\eta_1})}{K_1(r_w\sqrt{s/\eta_1})}, \tag{25}$$

$$\hat{P}_2^T = -\frac{\hat{q}\mu}{2\pi k_2 b_2 r_a \sqrt{s/\eta_2}} \frac{K_0\left(r_L\sqrt{s/\eta_2}\right)}{K_1\left(r_a\sqrt{s/\eta_2}\right)} \tag{26}$$

Let us define the following dimensionless groups,

$$s_D = \frac{s r_I^2}{\eta_1},\ \ q_D = q/Q_o,\ \ p_{D,i} = \frac{2\pi k_1 b_1 p_i^T}{Q_o\mu}\ (i=1,2),$$

$$\Omega_D = 2\pi k_1 b_1 \Omega,\ \ r_{D,x} = r_x / r_I\ \ (x = a,w,L,O),\ t_D = \frac{\eta_1}{r_I^2} t,\ \omega_D = \frac{\omega r_I^2}{\eta_1}$$

Then Eqs. (24)–(26) become

$$\hat{q}_D = \frac{\dfrac{-K_0(\sqrt{s_D})}{(s_D - i\omega_D) r_{D,w}\sqrt{s_D} K_1(r_{D,w}\sqrt{s_D})}}{\Omega_D + \dfrac{K_0(r_{D,a}\sqrt{s_D})}{r_{D,a}\sqrt{s_D} K_1(r_{D,a}\sqrt{s_D})} + \dfrac{K_0(r_{D,a}\sqrt{\alpha s_D})}{\beta r_{D,a}\sqrt{\alpha s_D} K_1(r_{D,a}\sqrt{\alpha s_D})}}, \tag{27}$$

$$\hat{P}_{D,1}^T = \frac{\hat{q}_D}{r_{D,a}\sqrt{s_D}} \frac{K_0(r_{D,L}\sqrt{s_D})}{K_1(r_{D,a}\sqrt{s_D})} + \frac{1}{r_{D,w}(s_D - i\omega_D)\sqrt{s_D}} \frac{K_0(r_{D,O}\sqrt{s_D})}{K_1(r_{D,w}\sqrt{s_D})}, \tag{28}$$

$$\hat{P}_{D,2}^T = -\frac{\hat{q}_D}{\beta r_{D,a}\sqrt{\alpha s_D}} \frac{K_0\left(r_{D,L}\sqrt{\alpha s_D}\right)}{K_1\left(r_{D,a}\sqrt{\alpha s_D}\right)}, \tag{29}$$

where $\alpha = \eta_1/\eta_2$ is the diffusivity ratio, and $\beta = k_2 b_2/(k_1 b_1)$ is transmissivity ratio. Because of the use of dimensionless groups, the dependence of leakage rate on Q_o disappears.

In general, the time domain solutions corresponding to Eqs. (27)–(29) need to be obtained by performing the inverse Laplace transform numerically. We show below that we can perform the frequency domain analysis for the current case without requiring the inverse Laplace transform. Let $\tilde{P}_{obs}(\omega)$ and $\tilde{P}_{inj}(\omega)$ be the Fourier transform of pressure buildups obtained at the observation well and injector, respectively. The frequency response function is defined as the ratio of $\tilde{P}_{obs}(\omega)$ to $\tilde{P}_{inj}(\omega)$

$$\mathcal{H}(\omega) = \frac{\tilde{P}_{obs}(\omega)}{\tilde{P}_{inj}(\omega)}. \tag{30}$$

Like the transfer function in time domain, $\mathcal{H}(\omega)$ provides a characterization of reservoir properties which, in turn, dictate how source strength attenuates with distance in a system. The latter characteristics can be quantified via the amplitude and phase of $\mathcal{H}(\omega)$

$$\Lambda = \left|\mathcal{H}(\omega)\right|,\ \Phi = \angle\mathcal{H}(\omega)\,. \tag{31}$$

Here Λ and Φ actually represent the amplitude attenuation and phase shift relative to the source. By definition, $\Lambda \le 1$. To normalize Φ, we take its modulo with respect to 2π and then divide the remainder by 2π. An advantage of Eq. (30) is that it allows the system responses to transient stimulations to be evaluated efficiently in terms of the periodic steady state responses to sinusoidal stimulations. Note that Eq. (30) is general and can be applied to any pair of observation well and injector pressure responses, which may be obtained either by conducting HPT in the field at multiple frequencies or by performing simulations. In the latter case, a forward model is used in lieu of monitoring data to generate simulated reservoir responses under HPT for detectability study.

Now we make use of the close connection between the Laplace transform and Fourier transform to obtain the steady periodic solutions directly from their Laplace domain solutions (Can and Ünal, 1988), by substituting *s* by $i\omega_D$ and making necessary adjustments. The results are

$$q_D = \frac{\dfrac{-K_0(\sqrt{i\omega_D})}{r_{D,w}\sqrt{i\omega_D}K_1(r_{D,w}\sqrt{i\omega_D})}}{\Omega_D + \dfrac{K_0(r_{D,a}\sqrt{i\omega_D})}{r_{D,a}\sqrt{i\omega_D}K_1(r_{D,a}\sqrt{i\omega_D})} + \dfrac{K_0(r_{D,a}\sqrt{\alpha i\omega_D})}{\beta r_{D,a}\sqrt{\alpha i\omega_D}K_1(r_{D,a}\sqrt{\alpha i\omega_D})}}, \tag{32}$$

$$p_{D,1}^T = \frac{q_D}{r_{D,a}\sqrt{i\omega_D}}\frac{K_0(r_{D,L}\sqrt{i\omega_D})}{K_1(r_{D,a}\sqrt{i\omega_D})} + \frac{1}{r_{D,w}\sqrt{i\omega_D}}\frac{K_0(r_{D,O}\sqrt{i\omega_D})}{K_1(r_{D,w}\sqrt{i\omega_D})}, \tag{33}$$

$$p_{D,2}^T = -\frac{q_D}{\beta r_{D,a}\sqrt{\alpha i\omega_D}}\frac{K_0\left(r_{D,L}\sqrt{\alpha i\omega_D}\right)}{K_1\left(r_{D,a}\sqrt{\alpha i\omega_D}\right)}. \tag{34}$$

Using Eq. (32)–(34), the frequency response function $\mathcal{H}_{leak}(\omega)$ can be calculated directly without the intermediate inverse Laplace transform step.

In the absence of leaks, the steady periodic pressure response in the reservoir can be expressed as,

$$p_{D,1} = \frac{K_0(\sqrt{i\omega'_D})}{r'_{D,w}\sqrt{i\omega'_D}K_1(r'_{D,w}\sqrt{i\omega'_D})}, \tag{35}$$

where $\omega'_D = \omega r_O^2/\eta_1$ and $r'_{D,w} = r_w/r_O$. Further, when $r_w \to 0$ Eq. (35) simplifies to

$$p_{D,1} = K_0(\sqrt{i\omega'_D})\,, \tag{36}$$

which is equivalent to the steady periodic solution show in (Rasmussen et al., 2003, Eq 6) by assuming a point source. For this case, the reservoir frequency response function can be expressed in terms of the steady periodic solutions given in Eq. (35)

$$\mathcal{H}_{noleak}(\omega'_D) = \frac{K_0(\sqrt{i\omega'_D})}{K_0(r'_{D,w}\sqrt{i\omega'_D})}. \tag{37}$$

The pair $\mathcal{H}_{noleak}$ and $\mathcal{H}_{leak}$ forms the basis of our pressure-based, frequency-domain leakage diagnosis tool. More specifically, if one or more leaks fall within the detection range of a HPT source, the power spectra of pressure responses will be modified and a visible deviation from the nominal reservoir frequency response function is expected. Again, $\mathcal{H}_{noleak}$ and $\mathcal{H}_{leak}$ may be obtained experimentally, numerically, or analytically.

Figure 2 shows that the amplitude of the frequency response function decreases monotonically as a function of the pulsing frequency. Shorter pulsing periods (i.e., higher frequencies) tend to attenuate the source energy much faster.

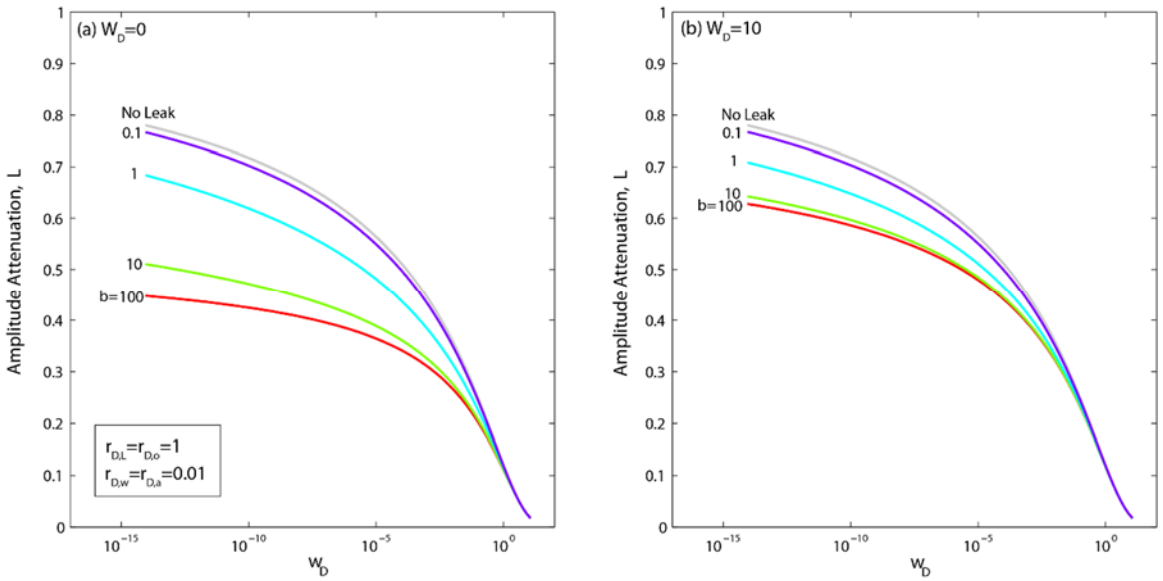

Figure 2. Amplitude attenuation as a function of transmissivity ratio (β) and dimensionless frequency for flow resistance (Ω).

Depending on the actual application setting, one of two approaches may be taken to generate the frequency-domain leakage diagnosis tool. Method 1 uses either field experiments or a forward model to conduct HPT at a number of pulsing periods, transforms the pressure response data into frequency domain responses by using fast Fourier transform (FFT), and then extracts the value of $\mathcal{H}$ at the fundamental frequency corresponding to each pulsing period (i.e., $2\pi / T_p$). The leads to a set of discrete points on a frequency response chart for leakage detection (see Section 3 for examples). Method 1 mimics the actual procedure that is likely to be used in practice, and pressure responses at the injector and observer are the only type of data required. The main advantage of Method 1 is it involves few assumptions and is the de facto option when the system is complex. Method 2 uses the analytical frequency domain solution provided herein to calculate the continuous frequency response functions and, thus, provides a validation of numerical procedures obtained using Method 1. Method 2 is a HPT-counterpart of the type-curve analyses often used in well testing literature. The main advantage of Method 2 is its computational efficiency. It can also

be used during scoping analysis to give quick estimates of expected deviations and to evaluate the range of detection for monitoring plan design.

Figure 3 presents a flow diagram for the proposed HPT procedure. We expect that the time-lapse approach is applicable as long as effective reservoir parameters in the testing zone do not change significantly between two back-to-back HPTs, such that the main source of the anomaly is leakage pathways not previously detected.

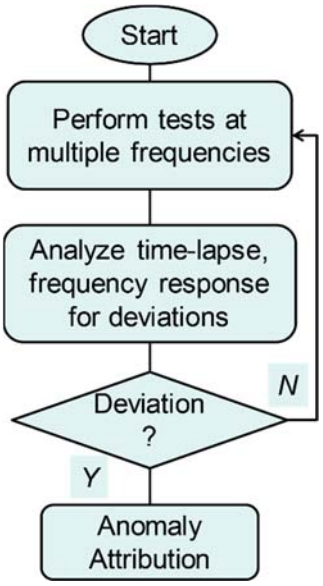

Figure 3. Illustration of the workflow of HPT-based leak detection.

2.2 Numerical validation

The single-phase semianalytical solution was verified numerically using the finite-element multiphysics software COMSOL. The results are shown in Figure 4, which suggests a good match between the semianalytical solution and the numerical model. We also performed multiphase numerical experiments to extend the semianlytical solution. In general, the results suggest similar trend as having been observed from single-phase experiments.

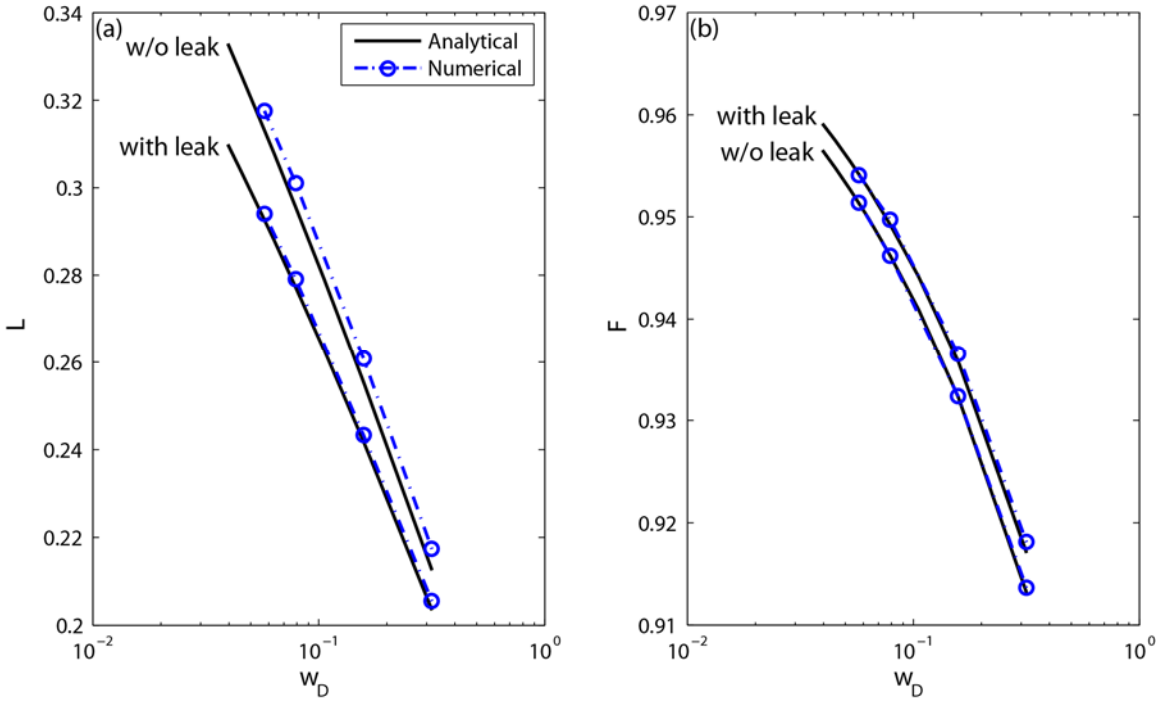

Figure 4. Numerical validation of the semianalytical solution shown in Section 2.1 for (a) amplitude attenuation and (b) phase shift.

3. TASK 3: LABORATORY EXPERIMENTS

The purpose of the sandbox experiments is to validate the concept of HPT in a controlled laboratory experiments. For this purpose, a meter-scale pressure vessel (referred to as stainless steel tank or SST below) was manufactured by UT's own machine shop.

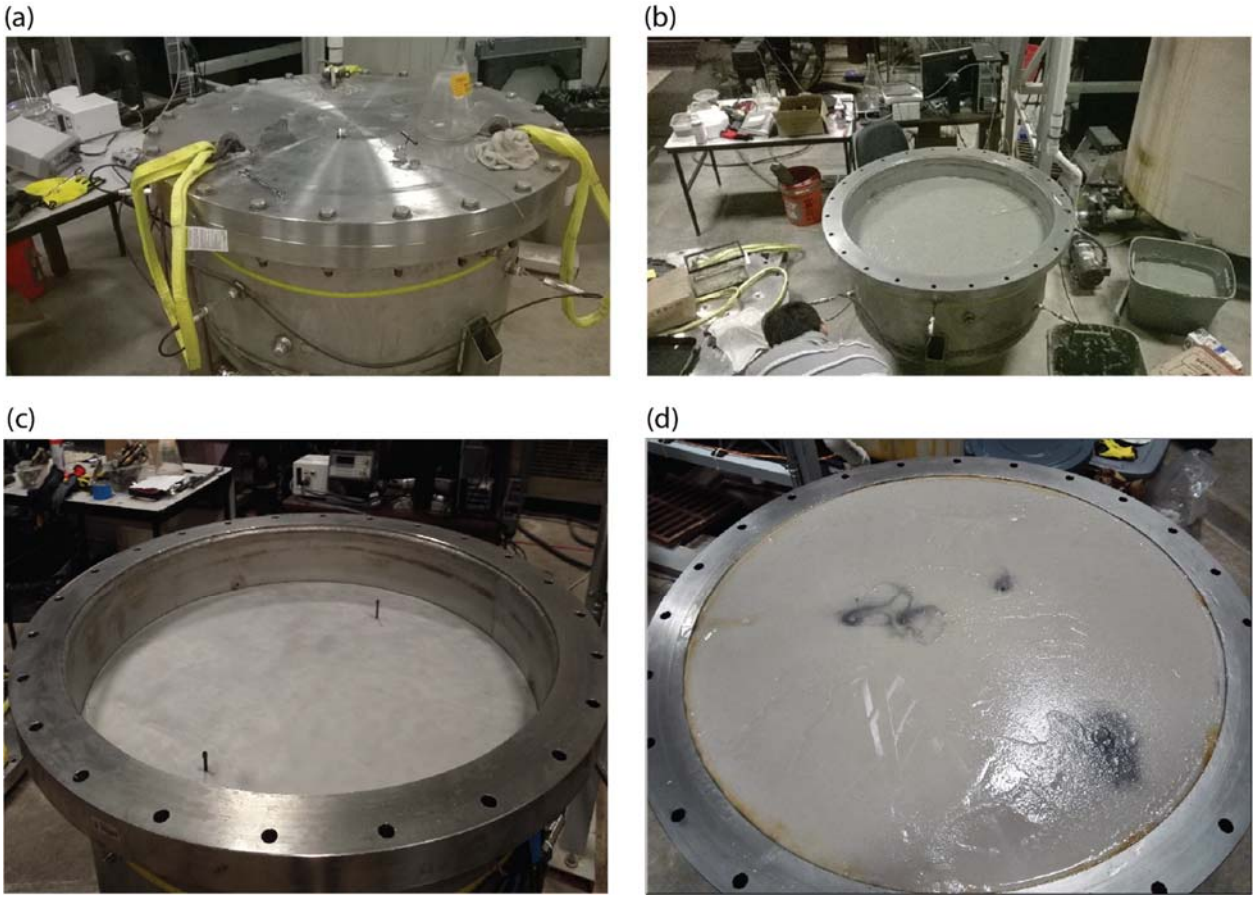

Figure 5. Stainless steel pressure vessel manufactured for the laboratory HPT tests: (a) view of the vessel; (b) experiment configuration using clay as confining layer; (c) experiment configuration using a thin metal plate as confining layer; (d) experiment showing failed clay confining layer (dark stain indicates the cracking of clay layer under pressure.

The SST tank mimics a mini 3D reservoir system with closed boundary. The tank body consists of a cylinder (inner diameter 1m, height 47 cm, rolled using 0.95cm-thick, SA-240 304 SST plate) and an inverted elliptical head (height 30cm, made using 0.95cm-thick, 304 SST) that are welded together. The lid of the tank was waterjet cut from a 5.72cm thick 304 SST plate, with the additional thickness designed to counter the extra stress imposed on the lid during injection (see Figure 5a). The design pressure of the tank is conservatively estimated to be 200 psi [1379 kpa]. An adjustable pressure release valve (McMaster-Carr adjustable brass relief valve with max pressure of 300psi [2068 kpa]) is installed at the bottom of the tank. The tank lid, which is removable using a fork lift, is attached to the tank body using uniformly spaced 1.27-cm hexhead bolts, with two rubber O-rings installed in between for water tightness.

Instrumentation ports were on the lid and around the tank wall. All the ports can also be used for simulating leakage pathways. The tank was thoroughly tested for water tightness before performing experiments.

HPT is implemented by using a hybrid piston-syringe pump (Car-May Novaspense™ Model 2-4, http://www.car-may.com/products.html, Berthoud, CO) and an arbitrary wave generator (Keysight 33210A 10MHz Function/Arb Waveform Gen., Santa Rosa, CA). The wave generator can modulate the injection rate to form sinusoidal, triangular, or square waves at different

magnitudes and frequencies. The tank is instrumented using 4 custom configured high-resolution pressure transducers (Omega Engineering, Stamford, CT) with a range of 250 psi [1724 kpa] and accuracy of ±0.03%. The pressure transducers are connected to a PC running Windows 7, via a data acquisition unit (OM-DAQ-USB-2401 data acquisition module, Omega Engineering, Stamford, CT). Figure 5a shows the pump and waver generator (white boxes on the table).

We performed a series of harmonic pulsing experiments under two main configurations. In the first configuration, the entire tank was filled with uniform sand (Accusill 30/40, AGSCO Corp, IL). The capacity of the tank is around 1 ton of sand when completely filled. The main purpose of this first configuration was to test the instrumentation and experimental procedures, especially with regard to displacement of entrapped air. During (wet) packing, the sand was slowly added and each layer was compacted, after which the tank was closed and CO_2 gas was injected from the bottom port of the tank to displace entrapped air bubbles. Each run typically starts from atmospheric pressure. Water is injected into the tank through oscillatory pumping until an upper pressure limit is reached, which is always kept below 150 psi [1034 kpa] to avoid pump damage. In principle, the net volume of injected water should be the same for the same total experimental time and injection rate, regardless of the pulsing frequency used. We verified this fact by keeping track of the water balance during experiments using scales. The consistency of oscillatory pumping frequency was also verified using a stop watch, which indicates that the pump is able to maintain consistent pumping cycles even under high pressures. For each experimental configuration, several runs were performed until the pressure increase became relatively linear at late times, indicating the gas phase was eliminated. Moreover, instead of releasing pressure when the tank is not used, it was found necessary to keep the tank under pressurized condition to keep the gas phase from forming (e.g., through exsolving from injected water).

After an experimental procedure was satisfactorily established, the tank was configured into a three-layer system, consisting a permeable injection layer, a low-permeability confining layer (i.e., caprock), and a permeable, above-zone layer. Such stylized three-layer systems have often been adopted in previous theoretical and numerical investigations for studying leakage from GCS repositories (Cihan et al., 2011; Nordbotten et al., 2004; Sun et al., 2015; Sun and Nicot, 2012). However, few studies have attempted to create such pressurized, layered systems in a laboratory setting.

Fabrication of the confining layer took several iterations. In the beginning, we used a thin layer of clay (bentonite) as the confining layer (see Figure 5b). Clay materials are commonly used in unconfined or low-pressure confined sandbox experiments to simulate flow barriers or confining beds. In our test, however, the clay confining layer quickly yielded after only a couple of runs, as suggested by the above-zone pressure transducers. Inspection after opening the tank lid also revealed several dark grey points, suggesting that the bentonite was flushed to the top through cracks ((Figure 5d)

Eventually, we formed the confining layer by covering a thin clay layer using a 0.635cm-thick aluminum divider that is caulked to the tank wall (Figure 5c). The thin clay layer was supported by another thin layer of fine sand (#100-140) from below, which is referred to as the transition zone.

The origin of the coordinates is located at the center of the bottom plane of the cylindrical tank body. The injection port is 0.125 m directly above the origin. Experiments were performed using pulsing periods of 30, 60, 90, 180, and 360 s, under both no-leak (baseline) and leak conditions. These ad hoc pulsing periods were chosen based on the pump's sensitivity to wave generator signals and on observed frequency responses. Sinusoidal injection rates were applied in all

experiments, with magnitudes varying between 0 and 40 ml/min. For the leak experiments, a leakage pathway was implemented by connecting the injection layer to the above-zone layer using a 0.0625cm [1/16 in] SST wireline that is controlled by a two-way needle valve to regulate the leak rate. All pressure transducer ports are deployed at their designated locations in the tank using 0.3175cm [1/8 in] SST tubing.

For reference, Table 1 lists the port locations (x, y, z coordinates) and their main uses during our experiments.

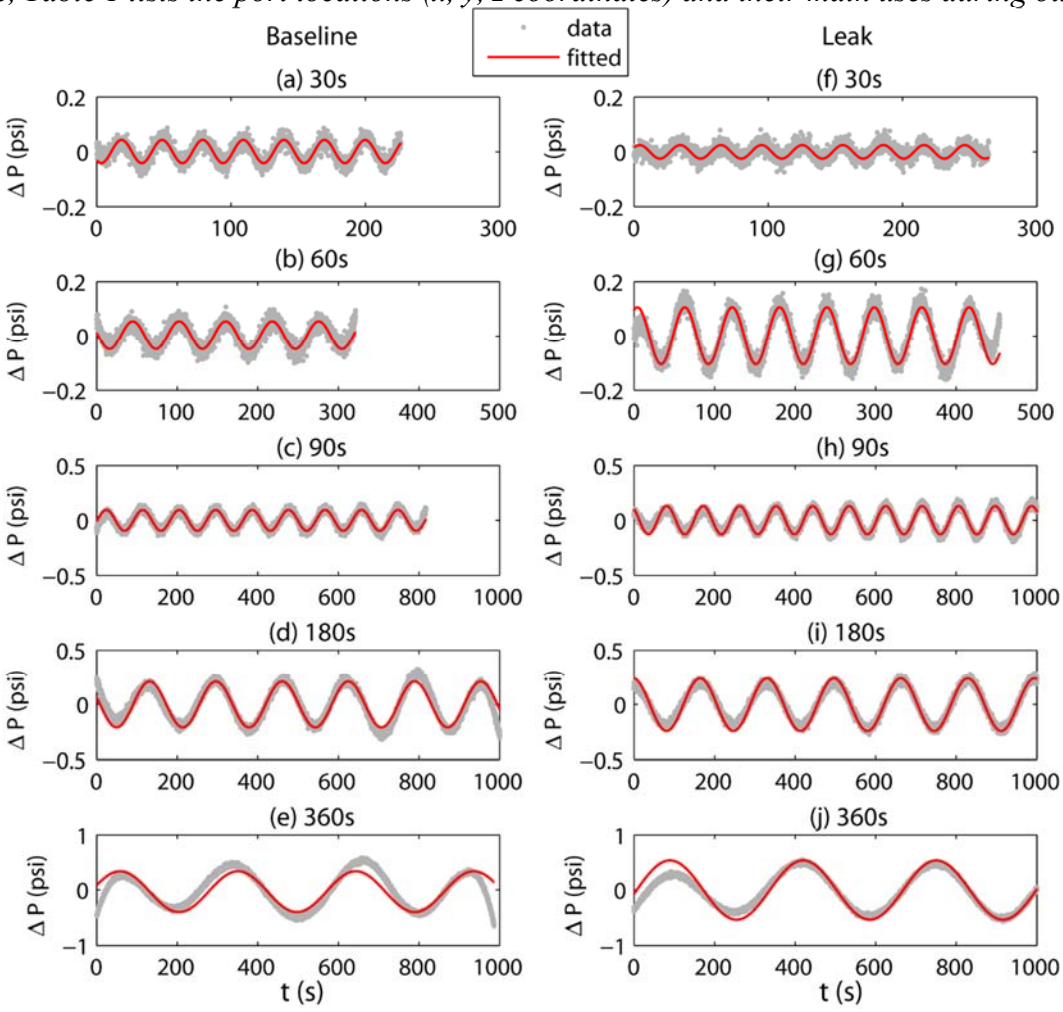

Figure 6 plots the observed pressure (with trend removed) time series at the pressure monitoring port C1 (located in the injection zone) during the baseline experiments. Figure 7 compares the baseline and leak experiments obtained from pressure ports A1 and A3 during the baseline and leak experiments (with trend removed). The pressure signals only show apparent sinusoidal patterns under leak conditions, indicating that the confining layer is functioning as expected during baseline experiments. Figure 8 compares the amplitudes of frequency response of nonleak experiments to leak experiments. Visible deviations can be observed.

Table 1. Port locations and their uses.

Port	x (cm)	y (cm)	z (cm)	Use
A1	38.97	22.5	37.5	Pressure (above zone)

A2	0	-50	37.5	Leak outlet
A3	-21.65	12.50	37.5	Pressure (above zone)
B3	-35.36	-35.36	25	Leak inlet
C1	0	45	12.5	Pressure (injection zone)
C2	0	0	12.5	Pressure (injection zone)
C3	0	0	12.5	Injector

In summary, we successfully created a mini reservoir in a laboratory environment. A large number of pressure experiments were conducted to validate the concept behind HPT-based leak detection. The results show that leaks would cause significant deviations from the baseline case where no leak is present. The results of the laboratory experiments were reported in a peer-reviewed journal article (Sun et al., 2017).

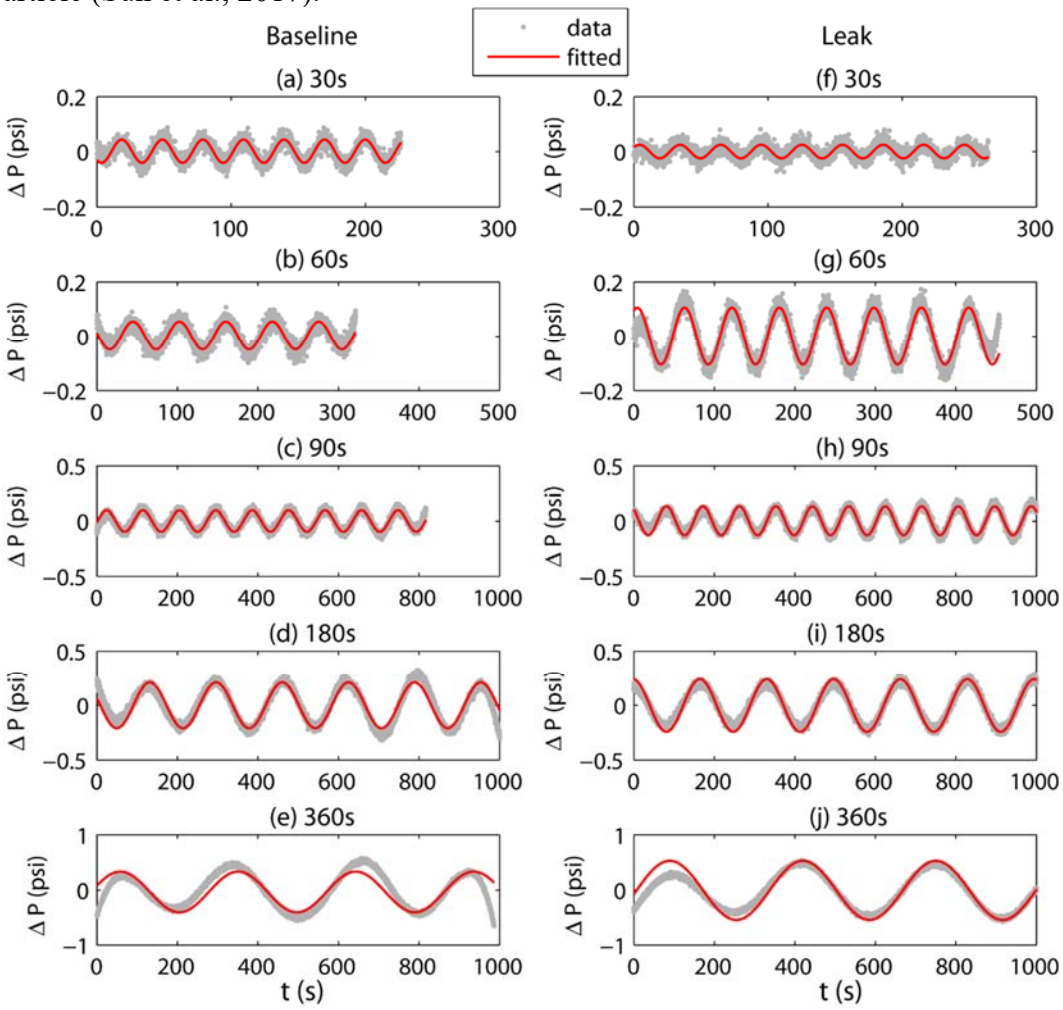

Figure 6. Monitored pressure results (after trend remove) at Port C1. (a)–(e): baseline pressure residuals obtained at pulsing periods of 30, 60, 90, 180, and 360s; (f)–(j): leak experiments pressure residuals obtained for the same pulsing periods. Data (grey dots) recorded at 0.1 s, and are fitted to 1-term Fourier series model (red solid line).

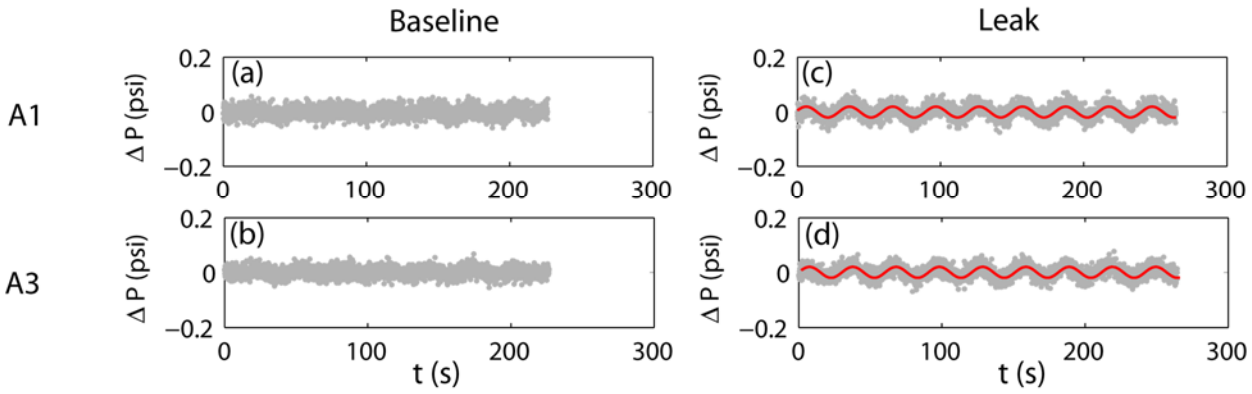

Figure 7. Pressure residuals obtained from above-zone pressure sensors A1 (top row) and A3 (bottom row) under baseline (a, c) and leak (b, d) condition, where solid lines correspond to models fitted using one-term Fourier series.

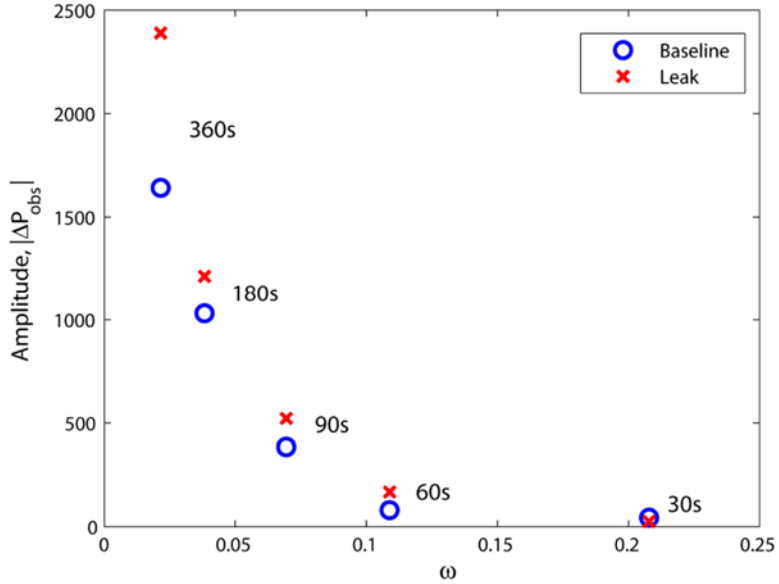

Figure 8. Amplitude vs. pulsing frequency diagram for all experiments. Pulsing periods are labeled on the plot and ranging from 30s to 360 s. The plot demonstrates that leak cases exhibit visible deviations from the nonleak cases.

4. TASK 4: INVERSION AND DATA ASSIMILATION ALGORITHM

The main purpose of Task 4 is to develop simulation tools. Under this task, the team has performed both forward modeling and inverse modeling required to analyzed and interpret experimental results. We developed leak source location procedure based on an algorithm originally presented in (Sun and Nicot, 2012). This algorithm, working together with the HPT, can be used to determine most probable leak location. Detailed description, as well as an example problem conducted using a COMSOL model, was presented in (Sun et al., 2015).

For the laboratory experiments, we developed a spectral space inversion procedure for estimating sandbox properties based on the pressure data time series. The results, demonstrated using the laboratory experiment data, suggest that the estimated properties are consistent with the known values. The details of the algorithm can be found in (Sun et al., 2017).

We developed single- and multiphase models to support the analysis of the field experiment data (see next section). The results are published in two papers (Min et al., 2018; Sun et al., 2016).

5. TASK 5: FIELD EXPERIMENTS

Field experiments were conducted at a conventional EOR field Cranfield, Mississippi, operated by Denbury Resources. Many of the past research and development activities at the Cranfield had been conducted at its Detailed Area of Study (DAS) site, which consists of three colinear wells, including one injector (CFU31-F1) and two monitoring wells (CFU31-F2 and CFU31-F3) (Figure 9Figure 9). These three wells will be referred to as F1, F2, and F3 in the remainder of this report. The surface separation distance between F1 and F2 is 69.8 m, and between F2 and F3 it is 29.9 m. The bottom-hole distance between F1 and F2 is 60 m; between F1 and F3 it is 93 m; and between F2 and F3 it is 33.5 m. F2 and F3 were completed with fiberglass casing to facilitate electrical resistance tomography (ERT) measurements and other well loggings during site characterization. All three wells are located just outside the oil field and completed in the water zone below the oil-water contact.

Figure 9. Areal view of the Detailed Area of Study at Cranfield, Mississippi (Lon: -91.141º, Lat: 31.564º), which consists of an injector (F1) and two monitoring wells (F2 and F3). During leak experiments, F3 was used as a "leaky" well. Locations of the flowback tank and trailer area are also labeled.

The field campaign for this project consisted of baseline and leak experiments, which were conducted sequentially. Before the field experiments, high-resolution permanent downhole gauges (Ranger Permanent Hybrid Digital Addressable Surface Read Out Gauge, Ranger Gauge Systems, Sugar Land, Texas, USA) were installed in well F2 and F3 on December 16–17, 2014. The control lines in each well consist of hybrid fiber-optic electrical cables encapsulated in 0.635-cm (¼-in) stainless steel tubing and were installed using a capillary injection unit through a lubricator and packoff. Resolution of the pressure gauge is 68.9 Pa (0.01 psi) and its data polling frequency is set to every 2 sec. As discussed below, these highly sensitive pressure gauges are necessary to detect small pressure anomalies. Records kept by our well management subcontractor (Sandia Technologies, LLC, Houston, Texas, USA) show that the depth of the downhole gauge assembly is 3,221.1 m (10,568 ft) in F2 and 3,222.0 m (10,571 ft) in F3. Ideally, the bottom-hole pressure (BHP) at F1 should also be monitored during the experiment to normalize the frequency response function (Section 2). However, it was not an option for this project. Thus, we mainly used the monitoring well data during analyses.

For the baseline, two sets of pulse testing experiments were performed on January 19 and January 20, 2015, one using a 90-min period and the other using a 150-min period. Each period starts with a shutin half cycle (50% of the time), followed by a constant-rate injection half cycle. These pulses were introduced to F1 by manually turning on/off the wellhead choke valve. F2 was used as the monitoring well in all experiments.

The actual pulse testing does not require additional equipment other than pressure gauges. However, because there is no known leakage pathway at the DAS site, for demonstration F3 was used to create an artificial leak by venting CO2 from its wellhead. For this purpose, a surface venting plumbing system was set up while the baseline experiments were being conducted. The venting system was used to control the leak rate and to connect to a flowback tank for properly disposing of reservoir fluids that flow out with the gas.

The leak experiments were repeated using the same pulsing periods as those used in the baseline tests, but with the controlled “leak” on all the time. The first leak experiment was started on January 23. Unfortunately, data communication with the downhole gauge in F2 was lost soon after the experiment started. A slickline service company was called in to replace the downhole gauge with a wireline memory gauge. Experiments then resumed one week later. A 90-min leak experiment was performed on January 30 and a 150-min leak experiment was performed the second day. Venting rate from F3 was fixed at 60 kg/min during two leak experiments, but sensitivity to smaller leak rates was also studied.

The 90-min baseline pulse testing was initiated at 11:10 on January 19 and lasted for 5 cycles. Each cycle consisted of a 45-min shutin period, followed by a 45-min period of constant-rate injection at 3,621 bbl/d (2.83x105 standard m^3/d), which is about twice the nominal injection rate (1,800 bbl/d) that had been used continuously at F1 for at least one month prior to our experiment. After the last shutin period of the experiment, the injection rate was set back to the nominal rate for the night. Before the experiment, the initial reservoir pressure was 4,718 psi (32.53 MPa). The formation factor corresponding to the reservoir pressure and temperature is 0.00317 reservoir bbl/bbl.

The baseline was repeated for the 150-min cycle on the second day (January 20) using the same injection rates. The test started at 8:25 and lasted for 4 cycles.

The 90-min leak experiment started at 8:30 on January 30 and venting of CO2 started at the same time. shows a typical scene from the leak experiment. The expansion of CO2 from liquid to gas phase absorbs heat. Thus, the pipeline to flowback tank is covered with frost under normal

conditions, as shown in the picture. However, when CO2 stream also has water and other impurities in it, ice forms inside the pipeline, eventually clogging the CO2 flow.

The 150-min leak experiment started at 8:30 on January 31. Venting was started at 8:10. The experiment went smoothly from the start until about 13:05 when the pipeline became frozen, causing the experiment to shut down for 20 min.

We applied the frequency-domain analysis on the pressure data collected from the field experiments during both baseline and leak experiments. Figure 11 plots the amplitude of response function as a function of the pulsing frequency ω. It can be seen that the leak experiments caused amplitude attenuation as compared to the baseline experiments. We also calculated the 95% confidence interval using a simple analytical solution (shaded area in Figure 11), which shows that with 95% confidence that the dots corresponding to the leak experiments are "leak" signals, instead of mainly reflecting parameter uncertainty.

More sophisticated 3D modeling was carried out to history match the pressure data collected from Cranfield experiments. The results, however, were mixed due to the limited dynamic information (e.g., CO2 saturation, initial condition, and actual injection rate during the experiments).

Detailed results of the field experiments can be found in (Sun et al., 2016) and the 3D simulation exercise in (Min et al., 2018).

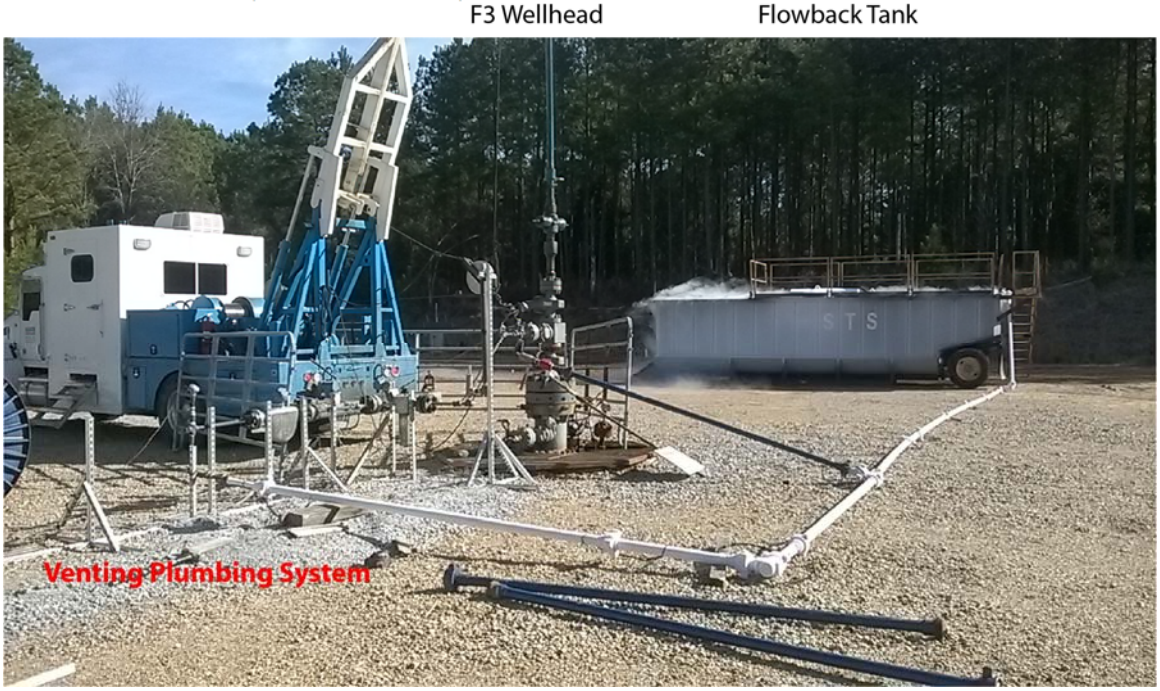

Figure 10. Scene from leak experiment in session, in which the venting pipeline is covered with frost, liquid flowback tank is in the far back, and a slickline pressure gauge is used to monitor downhole pressure.

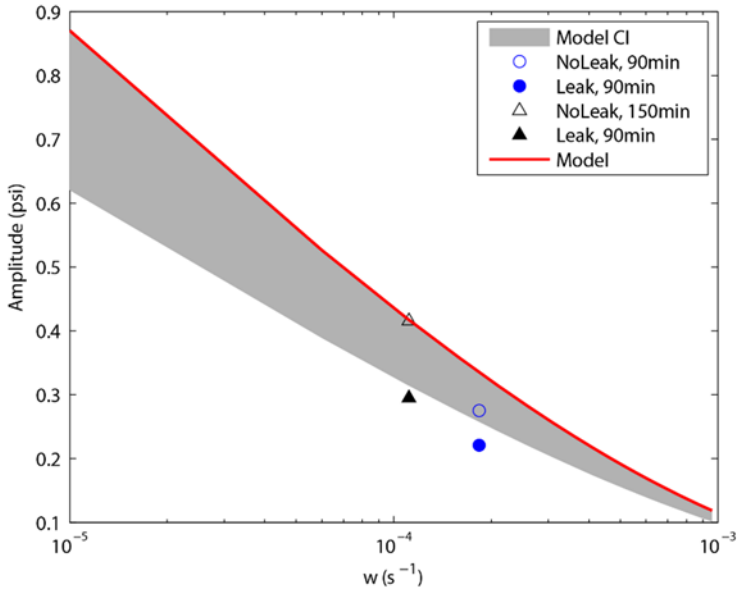

Figure 11. Leak (filled symbols) caused significant deviation in amplitudes of frequency response function as compared to the no-leak case (open symbols). Solid line is calculated using estimated reservoir parameter values and shaded area is formed by using lower 95% confidence bound.

6. TASK 6 INFORMATION DISSEMINATION

Under Task 6, we developed a web-based model for HPT scoping analysis. The module is implemented on a cloud-based virtual machine. The user can use the module to estimate the magnitude and frequency required for the pulsing experiments.

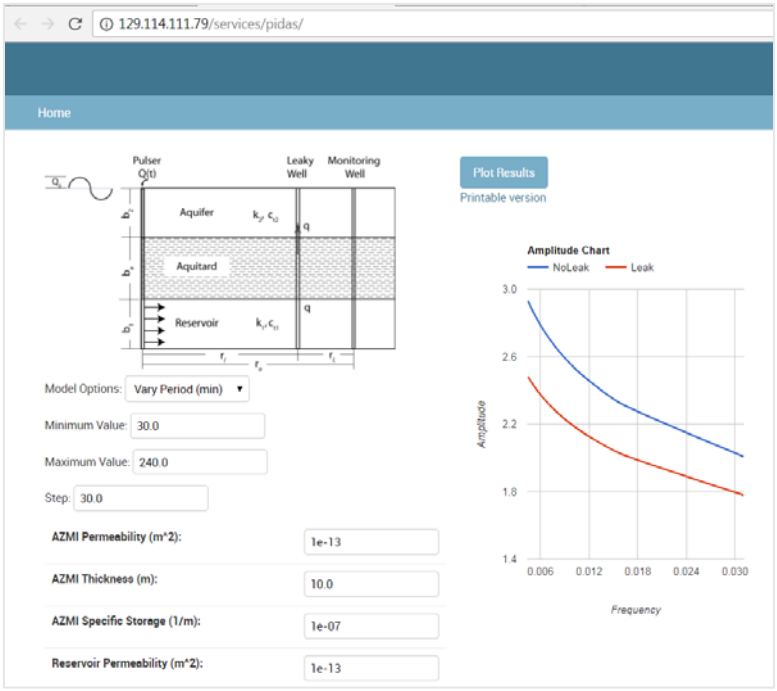

Figure 12. A web-based module for performing design of HPT experiments. The backend of the module is based on the semi-analytical solutions published in (Sun et al., 2015).

7. SUMMARY

In summary, a multi-faceted research was carried out under this project to perform proof-of-concept of a leakage probing technique based on harmonic pulse testing. All project tasks were performed according to the original Statement of Project Objectives. Pulse testing is similar to pressure interference tests often used in reservoir engineering for site characterization. The difference in this project is that we proposed to use the technology as a time-lapse monitoring tool. Pressure monitoring has been advocated as a cost-effective technology for early leakage diagnosis. A main benefit of using periodic injection rates is that the interference of reservoir noise is mitigated so that in-zone monitoring becomes possible, which is particularly useful when a quiescent above zone aquifer is not available for passive pressure monitoring. Accomplishments to date include

- We have established the theoretical basis and performed validation of the proposed pulse-testing-based leakage detection technique using a combination of modeling and experimental approaches.
- The technology was successfully demonstrated in a series of field tests performed at Cranfield, MS, an active CO2-EOR site.
- Dissemination of the technology is done by developing a web-based scoping analysis toolbox and by publishing a number of peer-reviewed journal papers

We have learned through this project that pulse-testing constitutes a viable, continuous, in-zone monitoring technology. The detection range of the technology is estimated to be around 500-1000m, depending on reservoir properties and pulsing frequencies (or period of each pulse). The technology proposed here should be deployed in a network fashion in which bottom-hole pressures at multiple monitoring wells, as well as the injectors, are continuously recorded and analyzed. From a best-management practice perspective, pulse testing should be recommended based on its cost effective nature.

8. PROJECT PUBLICATIONS

- Sun, A. Y., Kianinejad, A., Lu, J., & Hovorka, S. (2014). A frequency-domain diagnosis tool for early leakage detection at geologic carbon sequestration sites. Energy Procedia, 63, 4051-4061.
- Sun, A. Y., Lu, J., & Hovorka, S. (2015). A harmonic pulse testing method for leakage detection in deep subsurface storage formations. Water Resources Research, 51(6), 4263-4281.
- Sun, A. Y., Lu, J., B. Freifeld, A. Islam (2016). Using pulse testing for leakage detection in carbon storage reservoirs: A field demonstration. International Journal of Greenhouse Gas Control, 46(3), 215-227.
- Min, B., M. Wheeler, and A. Sun, Parallel Multi-Objective Optimization of Pulse Testing Using a Compositional Simulator for the Cranfield Gas Sequestration Project, SPE Reservoir Simulation Conference, Montgomery, Texas, February 20-22, 2017.
- Sun, A.Y., Lu, J., A. Islam. Laboratory validation of oscillatory pulse testing for leakage detection (2017). Journal of Hydrology, 548, 598-604
- Min, B., A. Y. Sun, M.F. Wheeler, H. Jeong (2018). Parallel multiobjective optimization for the coupled compositional/geomechanical modeling of pulse testing, Journal of Petroleum Science and Engineering, 170, 244-266.

REFERENCES

Ahn, S., Horne, R., 2010. Estimating permeability distributions from pressure pulse testing, SPE Annual Technical Conference and Exhibition.

Arsene, C.T.C., Gabrys, B., Al-Dabass, D., 2012. Decision support system for water distribution systems based on neural networks and graphs theory for leakage detection. Expert Systems with Applications, 39(18): 13214-13224. DOI:http://dx.doi.org/10.1016/j.eswa.2012.05.080

Avci, C.B., 1994. Evaluation of flow leakage through abandoned wells and boreholes. Water Resources Research, 30(9): 2565-2578.

Bernabé, Y., Mok, U., Evans, B., 2006. A note on the oscillating flow method for measuring rock permeability. International journal of rock mechanics and mining sciences, 43(2): 311-316.

Birkholzer, J.T. et al., 2011. Brine flow up a well caused by pressure perturbation from geologic carbon sequestration: Static and dynamic evaluations. International Journal of Greenhouse Gas Control, 5(4): 850-861. DOI:10.1016/j.ijggc.2011.01.003

Black, J., Kipp, K., 1981. Determination of hydrogeological parameters using sinusoidal pressure tests: a theoretical appraisal. Water Resources Research, 17(3): 686-692.

Can, S., Ünal, A., 1988. Transfer functions for nonlinear systems via Fourier-Borel transforms, NASA Report No. TM-100034,, NASA Ames Research Center, Moffett Field, CA.

Cardiff, M., Barrash, W., Kitanidis, P.K., 2013. Hydraulic conductivity imaging from 3-D transient hydraulic tomography at several pumping/observation densities. Water Resources Research, 49(11): 7311-7326.

Cihan, A., Zhou, Q., Birkholzer, J.T., 2011. Analytical solutions for pressure perturbation and fluid leakage through aquitards and wells in multilayered-aquifer systems. Water Resources Research, 47(10): W10504.

Ferrante, M., Brunone, B., 2003. Pipe system diagnosis and leak detection by unsteady-state tests. 1. Harmonic analysis. Advances in Water Resources, 26(1): 95-105.

Fokker, P.A., Verga, F., 2011. Application of harmonic pulse testing to water–oil displacement. Journal of Petroleum Science and Engineering, 79(3): 125-134.

Gringarten, A.C., 1986. Computer-Aided well test analysis, International Meeting on Petroleum Engineering. Society of Petroleum Engineers.

Gringarten, A.C., 1987. Type-curve analysis: what it can and cannot do. Journal of Petroleum Technology, 39(01): 11-13.

Gringarten, A.C., 2008. From straight lines to deconvolution: The evolution of the state of the art in well test analysis. SPE Reservoir Evaluation & Engineering, 11(1): 41-62.

Hollaender, F., Hammond, P.S., Gringarten, A.C., 2002. Harmonic testing for continuous well and reservoir monitoring. Paper presented at the SPE Annual Technical Conference and Exhibition, San Antonio, TX, September 29-October 2, 2002. SPE Journal, 77692.

Johnson, C.R., Greenkorn, R., Woods, E., 1966. Pulse-testing: a new method for describing reservoir flow properties between wells. Journal of Petroleum Technology, 18(12): 1,599-1,604.

Jung, Y., Zhou, Q., Birkholzer, J.T., 2013. Early detection of brine and CO_2 leakage through abandoned wells using pressure and surface-deformation monitoring data: Concept and demonstration. Advances in Water Resources(0). DOI:http://dx.doi.org/10.1016/j.advwatres.2013.06.008

Kuo, C., 1972a. Determination of reservoir properties from sinusoidal and multirate flow tests in one or more wells. Society of Petroleum Engineers Journal, 12(06): 499-507.

Kuo, C., 1972b. Determination of reservoir properties from sinusoidal and multirate flow tests in one or more wells. Old SPE Journal, 12(6): 499-507.

Lee, P.J., Vítkovský, J.P., Lambert, M.F., Simpson, A.R., Liggett, J.A., 2005. Frequency domain analysis for detecting pipeline leaks. Journal of Hydraulic Engineering, 131(7): 596-604.

Mahar, P.S., Datta, B., 2001. Optimal identification of ground-water pollution sources and parameter estimation. Journal of Water Resources Planning and Management, 127(1): 20-29.

Mandal, S.K., Chan, F.T., Tiwari, M., 2012. Leak detection of pipeline: An integrated approach of rough set theory and artificial bee colony trained SVM. Expert Systems with Applications, 39(3): 3071-3080.

Michalak, A.M., Kitanidis, P.K., 2004. Estimation of historical groundwater contaminant distribution using the adjoint state method applied to geostatistical inverse modeling. Water Resources Research, 40(8).

Min, B., Sun, A.Y., Wheeler, M.F., Jeong, H., 2018. Utilization of multiobjective optimization for pulse testing dataset from a CO 2-EOR/sequestration field. Journal of Petroleum Science and Engineering.

Mishra, P.K., Vessilinov, V., Gupta, H., 2013. On Simulation and Analysis of Variable-Rate Pumping Tests. Groundwater, 51(3): 469-473.

Mpesha, W., Gassman, S.L., Chaudhry, M.H., 2001. Leak detection in pipes by frequency response method. Journal of Hydraulic Engineering, 127(2): 134-147.

Nordbotten, J.M., Celia, M.A., Bachu, S., 2004. Analytical solutions for leakage rates through abandoned wells. Water Resour Res, 40(4). DOI:Artn W04204

Doi 10.1029/2003wr002997

Puust, R., Kapelan, Z., Savic, D., Koppel, T., 2010. A review of methods for leakage management in pipe networks. Urban Water Journal, 7(1): 25-45.

Rasmussen, T.C., Haborak, K.G., Young, M.H., 2003. Estimating aquifer hydraulic properties using sinusoidal pumping at the Savannah River site, South Carolina, USA. Hydrogeology Journal, 11(4): 466-482.

Sun, A.Y., Lu, J., Freifeld, B.M., Hovorka, S.D., Islam, A., 2016. Using pulse testing for leakage detection in carbon storage reservoirs: A field demonstration. International Journal of Greenhouse Gas Control, 46: 215-227.

Sun, A.Y., Lu, J., Hovorka, S., 2015. A harmonic pulse testing method for leakage detection in deep subsurface storage formations. Water Resources Research, 51(6): 4263-4281.

Sun, A.Y., Lu, J., Islam, A., 2017. A laboratory validation study of the time-lapse oscillatory pumping test for leakage detection in geological repositories. Journal of Hydrology, 548: 598-604.

Sun, A.Y., Nicot, J.-P., 2012. Inversion of pressure anomaly data for detecting leakage at geologic carbon sequestration sites. Advances in Water Resources, 44: 20-29.

Sun, A.Y., Painter, S.L., Wittmeyer, G.W., 2006. A constrained robust least squares approach for contaminant release history identification. Water Resour Res, 42(4). DOI:Artn W04414

Doi 10.1029/2005wr004312

Sun, A.Y., Zeidouni, M., Nicot, J.P., Lu, Z., Zhang, D., 2013. Assessing leakage detectability at geologic CO_2 sequestration sites using the probabilistic collocation method. Advances in Water Resources(56): 49-60.

Yang, Y.M. et al., 2011. Probabilistic design of a near-surface CO_2 leak detection system. Environmental Science & Technology, 45(15): 6380-6387.

Zeidouni, M., 2014. Analytical model of well leakage pressure perturbations in a closed aquifer system. Advances in Water Resources, 69: 13-22.

Zhang, Y., Oldenburg, C.M., Finsterle, S., 2010. Percolation-theory and fuzzy rule-based probability estimation of fault leakage at geologic carbon sequestration sites. Environmental Earth Sciences, 59(7): 1447-1459.